Constraints on scalar-induced gravitational waves up to third order from a joint analysis of BBN, CMB, and PTA data

Sai Wang [1,2,*] Zhi-Chao Zhao [3] and Qing-Hua Zhu [4,2]

[1]*Theoretical Physics Division, Institute of High Energy Physics, Chinese Academy of Sciences, Beijing 100049, China*
[2]*University of Chinese Academy of Sciences, Beijing 100049, China*
[3]*Department of Applied Physics, College of Science, China Agricultural University, Qinghua East Road, Beijing 100083, China*
[4]*CAS Key Laboratory of Theoretical Physics, Institute of Theoretical Physics, Chinese Academy of Sciences, Beijing 100190, China*

(Received 19 September 2023; accepted 23 January 2024; published 26 February 2024)

Recently, strong evidence for a gravitational-wave background has been reported by collaborations of pulsar timing arrays (PTAs). In the framework of scalar-induced gravitational waves, we concurrently investigate the second- and third-order gravitational waves by jointly analyzing PTA data alongside big-bang nucleosynthesis and cosmic microwave background datasets. We determine the primordial curvature spectral amplitude as $0.021 < A_\zeta < 0.085$ and the spectral peak frequency as $10^{-7.3}\ \mathrm{Hz} < f_* < 10^{-6.3}\ \mathrm{Hz}$ at a 95% confidence interval, pointing towards a mass range for primordial black holes of $10^{-4.5} M_\odot < m_{\mathrm{PBH}} < 10^{-2.5} M_\odot$. Our findings suggest that third-order gravitational waves contribute more significantly to the integrated energy density than the second-order ones when $A_\zeta \gtrsim 0.06$. Furthermore, we expect future PTA projects to validate these findings and provide robust means to investigate the genesis and evolution of the universe, especially inflation.

DOI: 10.1103/PhysRevResearch.6.013207

I. INTRODUCTION

The theory of scalar-induced gravitational waves (SIGWs) [1–6] has been proposed to interpret the substantial evidence of nano-Hertz gravitational-wave background (GWB) signals reported by several pulsar timing array (PTA) collaborations [7–10]. It has been suggested to offer a better fit than the astrophysical interpretation in the context of super-massive black hole (SMBH) binaries [11–13]. Subsequent related studies are detailed in Refs. [14–23]. Significant constraints have been imposed on the enhanced primordial curvature power spectrum at small scales which are unreachable for conventional probes, such as the cosmic microwave background (CMB) that is sensitive to physics on the largest observable universe scales [24]. However, these studies have solely considered second-order gravitational waves, disregarding contributions from higher-order ones.

In addition to the direct measurements of SIGWs from the PTA probe, early-universe probes offer indirect constraints on the integrated SIGW spectrum [25]. Given that SIGWs behave like radiation in the universe, their energy can alter the growth of cosmological density perturbations and the universe's expansion rate at the time of decoupling. Consequently, the CMB probe is sensitive to the integrated SIGW spectrum [26,27]. Simultaneously, the success of big-bang nucleosynthesis (BBN) theory can limit the number of relativistic species at the nucleosynthesis epoch. Therefore the BBN probe is sensitive to the energy of SIGWs [28]. Both probes independently measure cosmological GWBs of frequency bands above $10^{-10}\,\mathrm{Hz}$ but are insensitive to other GWBs produced due to astrophysical processes in the late universe.

In this study we simultaneously consider second- and third-order gravitational waves and explore joint constraint on them from BBN, CMB, and PTA datasets. Previous research on third-order gravitational waves is documented in Refs. [29,30]. We will demonstrate that they dominate the SIGW's energy density if the primordial curvature spectral amplitude exceeds $\mathcal{O}(0.06)$. We will also illustrate that they do not significantly alter the PTA bound but cause substantial changes in the BBN and CMB bounds. Consequently, the joint constraint will also experience significant alterations. Moreover, we will explore these possibilities and potential future improvements.

II. SCALAR-INDUCED GRAVITATIONAL WAVES

Adhering to the conventions of Ref. [31], we adopt the perturbed, spatially flat Friedman-Robertson-Walker metric in Newtonian gauge, specifically,

$$\begin{aligned} \mathrm{d}s^2 = a^2\big\{&-(1+2\phi^{(1)}+\phi^{(2)})\mathrm{d}\eta^2 + V_i^{(2)}\mathrm{d}\eta\mathrm{d}x^i \\ &+\big[(1-2\psi^{(1)}-\psi^{(2)})\delta_{ij}+\tfrac{1}{2}h_{ij}^{(2)}+\tfrac{1}{6}h_{ij}^{(3)}\big]\mathrm{d}x^i\mathrm{d}x^j\big\}, \end{aligned} \tag{1}$$

where the superscript $^{(n)}$ signifies the nth-order perturbations, ϕ and ψ represent scalar perturbations, V_i indicates transverse vector perturbations, and h_{ij} denotes transverse-traceless tensor perturbations.

Tensor perturbations h_{ij} induced by the linear scalar perturbations are referred to as SIGWs. Second-order gravitational

*Corresponding author: wangsai@ihep.ac.cn

waves have been investigated in the literature [1–6], and we follow the conventions of Ref. [6]. As shown in Appendix A, the equation of motion for third-order gravitational waves is [30]

$$h_{ij}^{(3)''} + 2\mathcal{H}h_{ij}^{(3)'} - \Delta h_{ij}^{(3)} = -12\Lambda_{ij}^{lm}\mathcal{S}_{lm}^{(3)}, \tag{2}$$

where $\mathcal{H}$ is conformal Hubble parameter, Δ is a Laplacian, Λ_{ij}^{lm} is the transverse-traceless operator, and $\mathcal{S}_{lm}^{(3)}(\eta, \boldsymbol{x})$ denotes source terms, as expressed in Eq. (A2). Leveraging the two-point correlators of $h_{ij,\boldsymbol{k}}^{(3)}$, i.e., $\langle h_{ij,\boldsymbol{k}}^{(3)} h_{ij,\boldsymbol{k}'}^{(3)}\rangle = 2(2\pi)^3\delta(\boldsymbol{k}+\boldsymbol{k}')(2\pi^2)k^{-3}\mathcal{P}_h^{(3)}(k)$, we get the power spectrum for third-order gravitational waves, i.e.,

$$\begin{aligned}\mathcal{P}_h^{(3)}(k,\eta) = {} & \frac{k^3}{32\pi^2}\left(\frac{4}{9}\right)^3 \sum_{*,**}\int \frac{\mathrm{d}^3p\mathrm{d}^3q}{|\boldsymbol{k}-\boldsymbol{p}|^3|\boldsymbol{p}-\boldsymbol{q}|^3|\boldsymbol{q}|^3}\{\mathcal{P}_\zeta(|\boldsymbol{k}-\boldsymbol{p}|)\mathcal{P}_\zeta(|\boldsymbol{p}-\boldsymbol{q}|)\mathcal{P}_\zeta(q) \\ & \times \mathbb{P}_{*,ij}(\boldsymbol{k},\boldsymbol{p},\boldsymbol{q})I_*^{(3)}(|\boldsymbol{k}-\boldsymbol{p}|,|\boldsymbol{p}-\boldsymbol{q}|,|\boldsymbol{q}|,|\boldsymbol{p}|,k,\eta)[\mathbb{P}_{**,ij}(-\boldsymbol{k},-\boldsymbol{p},-\boldsymbol{q})I_{**}^{(3)}(|\boldsymbol{k}-\boldsymbol{p}|,|\boldsymbol{p}-\boldsymbol{q}|,|\boldsymbol{q}|,|\boldsymbol{p}|,k,\eta) \\ & + (\boldsymbol{p}\to\boldsymbol{p}-\boldsymbol{q}) + (\boldsymbol{p}\to\boldsymbol{k}-\boldsymbol{q},\boldsymbol{q}\to\boldsymbol{k}-\boldsymbol{p}) + (\boldsymbol{p}\to\boldsymbol{k}-\boldsymbol{q},\boldsymbol{q}\to\boldsymbol{p}-\boldsymbol{q}) \\ & + (\boldsymbol{p}\to\boldsymbol{k}-\boldsymbol{p}+\boldsymbol{q}) + (\boldsymbol{p}\to\boldsymbol{k}-\boldsymbol{p}+\boldsymbol{q},\boldsymbol{q}\to\boldsymbol{k}-\boldsymbol{p})]\},\end{aligned} \tag{3}$$

where we introduce the quantities $\mathbb{P}_*(\boldsymbol{k},\boldsymbol{p},\boldsymbol{q})$ and the kernel functions $I_*^{(3)}(p_1,p_2,p_3,p_4,k,\eta)$ in Appendix A, the subscripts $_*$ and $_{**}$ denoting different sources of third-order gravitational waves, i.e., in terms of $(\phi^{(1)})^3$, $\phi^{(1)}\psi^{(2)}$, $\phi^{(1)}V_i^{(2)}$, $\phi^{(1)}h_{ij}^{(2)}$.

Regarding the primordial black hole (PBH) formation, there should be a large-amplitude peak on the power spectrum of primordial curvature perturbations [32–34]. Inflation models with sound speed resonance can generate a nearly monochromatic spectrum [35–40]. For simplicity, we consider a δ-function spectrum

$$\mathcal{P}_\zeta(k) = A_\zeta k_*\delta(k-k_*), \tag{4}$$

where A_ζ is the amplitude and k_* is the pivot wave number. The energy-density fraction spectrum of SIGWs is defined as $\Omega_{\mathrm{GW}}(k,\eta) = 2\pi G\langle\partial_l h_{ij}\partial_l h_{ij}\rangle/[a^2\rho_c(\eta)]$ [6], where $h_{ij} \equiv (1/2)h_{ij}^{(2)} + (1/6)h_{ij}^{(3)}$, and ρ_c is critical density at conformal time η. We determine it as

$$\Omega_{\mathrm{GW}}(k,\eta) = \frac{A_\zeta^2}{24}\left(\frac{k}{\mathcal{H}}\right)^2\left[\mathcal{P}_h^{(2)}(k,\eta) + \frac{A_\zeta}{9}\mathcal{P}_h^{(3)}(k,\eta)\right], \tag{5}$$

where the power spectrum of second-order gravitational waves, $\mathcal{P}_h^{(2)}(k,\eta)$, is calculated in pioneers' works [1–6], and the power spectrum of third-order ones, $\mathcal{P}_h^{(3)}(k,\eta)$, is shown in Eq. (3). Since gravitational waves behave like radiations, the energy-density fraction spectrum in the present universe is [41]

$$\Omega_{\mathrm{GW},0}(k) = \Omega_{\mathrm{r},0}\left[\frac{g_{*,\rho}(T)}{g_{*,\rho}(T_{\mathrm{eq}})}\right]\left[\frac{g_{*,s}(T_{\mathrm{eq}})}{g_{*,s}(T)}\right]^{\frac{4}{3}}\Omega_{\mathrm{GW}}(k,\eta), \tag{6}$$

where the physical energy-density fraction of radiations in the present universe is $\Omega_{\mathrm{r},0}h^2 \simeq 4.2\times10^{-5}$, with $h = 0.6766$ being the dimensionless Hubble constant [42], a subscript $_{\mathrm{eq}}$ denotes cosmological quantities at the epoch of matter-radiation equality, and both $g_{*,\rho}$ and $g_{*,s}$ stand for the effective relativistic specifies in the universe [43]. Moreover, cosmic temperature T is related with k, i.e.,

$$\frac{k}{\mathrm{nHz}} = 83.25\left(\frac{T}{\mathrm{GeV}}\right)\left[\frac{g_{*,\rho}(T)}{106.75}\right]^{\frac{1}{2}}\left[\frac{g_{*,s}(T)}{106.75}\right]^{-\frac{1}{3}}. \tag{7}$$

It should be emphasized that the contributions from the third-order gravitational waves become significant on the small scales $k \gg k_*$. This is primarily due to the additional enhancement in their power spectrum originated from resonance of the higher-order perturbations at late times. On the other hand, for the large scales $k \ll k_*$, the contributions from the third-order gravitational waves can be neglected because their power spectrum is highly suppressed compared to that of the second-order gravitational waves.

The theoretical predictions of the aforementioned spectrum are depicted in Fig. 1. In this case we set the model parameters to $A_\zeta = 0.1$ (solid curves) and $A_\zeta = 0.01$ (dashed curves). The spectrum of the second-order gravitational waves is represented in blue, while the combined spectrum of both the second- and third-order gravitational waves is shown in red. In comparison to the second-order gravitational waves,

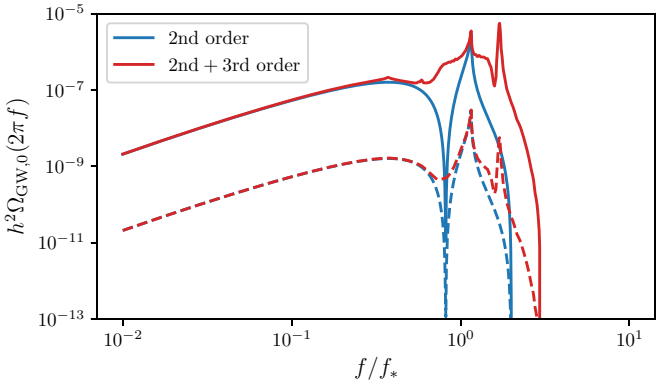

FIG. 1. This figure contrasts the energy-density spectra of second order (blue) with those of both second and third orders (red). The model parameters provided are $A_\zeta = 0.1$ (solid) and $A_\zeta = 0.01$ (dashed).

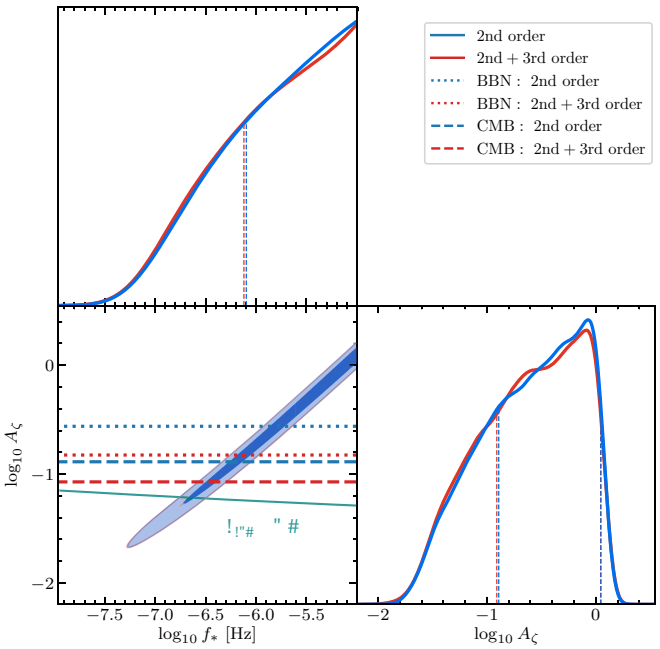

FIG. 2. The posteriors for the model parameters A_ζ and f_* derived from the NG15 PTA dataset (contours), in addition to the BBN (thick dotted lines) and CMB (thick dashed lines) upper limits on A_ζ. For the one-dimensional posteriors, the 68% confidence intervals are indicated by thin dashed lines. Deep green line denotes $f_{\rm PBH} = 1$, indicating that all of dark matter is composed of PBHs [12].

the third-order gravitational waves primarily contribute to the spectrum around the peak frequencies.

III. JOINT CONSTRAINTS

It is known that the PTA probe is directly sensitive to the energy density of SIGWs. Following the methodology of Ref. [12], we examine the parameter space by conducting a Bayesian analysis over the NANOGrav 15-year (NG15) dataset [9]. The priors of $\log_{10}(f_*/{\rm Hz})$ and $\log A_\zeta$ are uniformly set within the intervals of $[-11,-5]$ and $[-3,1]$, respectively. In fact, our results are robust with respect to priors. Here, we neglect the very likely presence of an astrophysical foreground, which has been considered in Refs. [44,45].

We consider two scenarios related to SIGWs. The first scenario (scenario I) includes only the second-order gravitational waves, while the second scenario (scenario II) incorporates both the second- and third-order gravitational waves. For both scenarios we derive the posteriors of f_* and A_ζ, which are illustrated in Fig. 2. Statistically, it is challenging to differentiate between the two scenarios since their posteriors nearly overlap. We conclude that the third-order gravitational waves, when being compared with the second-order ones, have negligible impact on the interpretation of the observed PTA signal in terms of SIGWs.

The BBN and CMB probes are indirectly sensitive to the energy density of SIGWs.[1] Specifically, they are sensitive only to the integrated energy-density fraction, as described by

$$\int_{k_{\rm min}}^{\infty} {\rm d}\ln k\, h^2 \Omega_{{\rm GW},0}(k) < 1.3\times10^{-6}\left(\frac{N_{\rm eff}-3.046}{0.234}\right), \quad (8)$$

where $k_{\rm min} = 2\pi f_{\rm min}$ sets the lower bound of the integral, and $N_{\rm eff}$ represents the number of relativistic species. As $f_{\rm min}$ is dependent on the physical process that occurred during the epochs of BBN and CMB formation, we adopt $f_{\rm BBN} \simeq 1.5\times10^{-11}$ Hz for BBN and $f_{\rm CMB} \simeq 3\times10^{-17}$ Hz for CMB [24]. According to the Planck 2018 CMB plus BAO dataset [42], the right-hand side of Eq. (8) equals 2.9×10^{-7} [27], resulting in an upper limit of $A_\zeta \leqslant 0.130$ for scenario I and $A_\zeta \leqslant 0.085$ for scenario II. In contrast, for BBN the right-hand side equals 1.3×10^{-6} [28], yielding an upper limit of $A_\zeta = 0.275$ for scenario I and $A_\zeta = 0.150$ for scenario II. These upper limits are illustrated in Fig. 2. Though the contours are almost the same as those in Ref. [12], the BBN and CMB upper bounds would significantly alter the posteriors via reducing a large portion of the posteriors. This indicates the importance of the data combination.

The results from the joint analysis are as follows. In both scenarios the parameter region inferred from the NG15 data is notably refined by the inclusion of the BBN and CMB data. The permissible upper limit on A_ζ is somewhat smaller in scenario II than in scenario I, highlighting the significance of third-order gravitational waves. Starting from the peak of the posterior, we derive the combined constraints on A_ζ and f_* as

$$0.021 < A_\zeta < 0.085, \quad (9)$$

$$5.0\times10^{-8}{\rm Hz} < f_* < 5.0\times10^{-7}{\rm Hz}, \quad (10)$$

at the 95% confidence level. To our knowledge, these findings represent the state-of-the-art and most stringent constraints on the model parameters.

It should be noted that when $A_\zeta \gtrsim 0.06$, the third-order gravitational waves contribute more to the integrated energy density than the second-order ones. This outcome suggests that the third-order gravitational waves cannot be disregarded in the data analysis of BBN and CMB.

Taking into account both the second- and third-order gravitational waves, we also find that the CMB bound, denoted by the dashed red line in Fig. 2, is comparable to the deep green line, which indicates all of dark matter to be composed of PBHs, i.e., $f_{\rm PBH} = 1$ [12]. There may be a risk of overproducing PBHs. However, the allowed maximum peak amplitude of the power spectrum is $A_\zeta \simeq 0.058$, an amplitude making the third-order contribution as nearly equal as the second-order one. Therefore it is important to take into account the third-order gravitational waves in our analysis.

IV. ANTICIPATED CONSTRAINTS

It is anticipated that the energy-density fraction spectrum of SIGWs, and subsequently the power spectrum of primordial curvature perturbations, will be potentially measured by the Square Kilometre Array (SKA) [47–49], μAres [50], Laser Interferometer Space Antenna [51,52], big bang

[1]Dr. Carlo Tasillo tells us via email that they have studied phase-transition gravitational waves by jointly analyzing the BBN, CMB, and NANOGrav 12.5-year data [46].

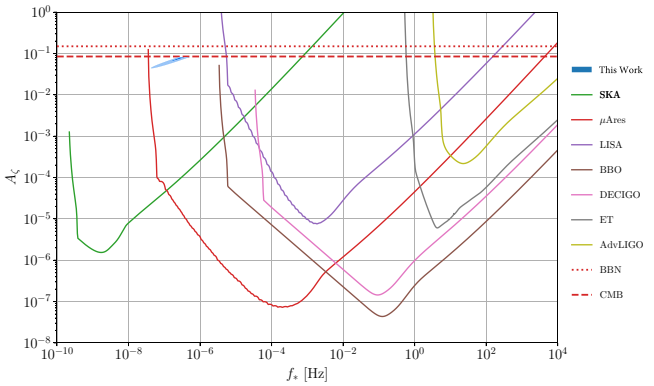

FIG. 3. Projected constraint capabilities of future gravitational-wave detection projects. The allowable parameter region inferred from Fig. 2, as well as the upper limits from present BBN and CMB observations, are also displayed for comparison. Here, we set SNR = 1 and neglect the very likely presence of an astrophysical foreground.

observer [53,54], Deci-Hertz Interferometer Gravitational Wave Observatory [55,56], Einstein Telescope [57], and Advanced LIGO and Virgo [58–60]. Complementing CMB, which is sensitive to the earliest stages of inflation, gravitational-wave probes offer the capability to investigate the physics of the early universe that occurred during later stages of inflation. Conducting multiband gravitational-wave observations, we expect to explore the origin and evolution of the universe throughout the entire inflationary era.

Following Ref. [61], we examine this subject. During a GWB search, if neglecting the very likely presence of an astrophysical foreground, the optimal signal-to-noise ratio is defined as [62]

$$\mathrm{SNR}^2 = n_{\mathrm{det}} T_{\mathrm{obs}} \left(\frac{3H_0^2}{2\pi^2}\right)^2 \int_{f_{\mathrm{l}}}^{f_{\mathrm{u}}} \left[\frac{\Omega_{\mathrm{GW},0}(f)}{f^3 S_n^{\mathrm{eff}}(f)}\right]^2 \mathrm{d}f, \qquad (11)$$

where n_{det} represents the number of detectors, T_{obs} is the observation duration, the frequency band extends from f_{l} to f_{u}, and S_n^{eff} denotes the effective noise power spectral density of the detector network. Here, $H_0 = 100h$ km/s/Mpc is the Hubble constant. For the aforementioned experiments, we employ the setups summarized in Table 2 of Ref. [44].

Requiring SNR = 1, we illustrate the anticipated constraint contours in the A_ζ–f_* plane for SKA in Fig. 3. The allowable parameter region (blue shaded contours) inferred from this study is presented for comparison. Notably, we find that our inferred contours can be further tested with SKA and μAres. We note superb performance in measuring the primordial curvature spectral amplitude, i.e., $A_\zeta \sim 10^{-6}$ for PTA projects, $A_\zeta \sim 10^{-8}$ for space-borne projects, and $A_\zeta \sim 10^{-5}$ for ground-based projects. The high sensitivities should enable us to explore the early universe more comprehensively.

V. CONCLUSION AND DISCUSSION

In this study we have delved into the gravitational waves induced by scalar perturbations, up to the third order, by scrutinizing recent PTA datasets in conjunction with BBN and CMB data. We have calculated the energy-density spectrum of SIGWs up to third order. Through the analysis of the joint datasets of BBN, CMB, and PTA, we inferred the allowable parameter region, which is depicted in Fig. 2. The inferred constraints on A_ζ and f_* are presented in Eqs. (9) and (10).

Interestingly, we found that the third-order gravitational waves could contribute more to the integrated energy density than the second-order ones when the primordial curvature spectral amplitude A_ζ exceeds approximately 0.06. This finding underscores the importance of third-order gravitational waves in our joint data analysis.

As illustrated in Fig. 3, we anticipated that the energy-density fraction spectrum of scalar-induced gravitational waves, and subsequently the power spectrum of primordial curvature perturbations, will be potentially measured by future gravitational-wave experiments, which should enable us to explore the early universe more comprehensively and further test the predictions of our study. Our findings represent a significant step forward in our understanding of the universe, particularly in relation to cosmic inflation.

The next-generation CMB experiments, e.g., CMB-S4 [63], Simons Observatory [64], and LiteBIRD [65], are expected to reach better sensitivity that would lead to improvements of the present CMB upper limits on A_ζ, also indicating potential improvements of the best bound inferred in our current work.

Our results also suggest a mass range for PBHs (see reviews in Ref. [66]) of $10^{-4.5} M_\odot < m_{\mathrm{PBH}} < 10^{-2.5} M_\odot$, assuming the observed PTA signal is interpreted as originating from SIGWs [14–17,67–75]. Notably, this mass range could account for the evidence for Planet 9 in the Outer Solar System [76–82].

ACKNOWLEDGMENTS

S.W. is partially supported by the National Natural Science Foundation of China (Grant No. 12175243), the National Key R&D Program of China (No. 2023YFC2206403), the Science Research Grants from the China Manned Space Project (No. CMS-CSST-2021-B01), and the Key Research Program of the Chinese Academy of Sciences (Grant No. XDPB15). Z.C.Z. is supported by the National Key Research and Development Program of China (Grant No. 2021YFC2203001) and the National Natural Science Foundation of China (Grant No. 12005016). Z.Q.Z. is supported by the National Nature Science Foundation of China (Grant No. 12305073). This work is supported by the High-Performance Computing Platform of China Agricultural University.

APPENDIX: ESSENTIAL FORMULAS

Once the perturbed metric in Eq. (2) is known, we derive the equations of motion for SIGWs from the Einstein's equations in a hierarchical approach. For third-order gravitational waves we have [30]

$$h_{ij}^{(3)''}(\eta, \boldsymbol{x}) + 2\mathcal{H} h_{ij}^{(3)'}(\eta, \boldsymbol{x}) - \Delta h_{ij}^{(3)}(\eta, \boldsymbol{x}) = -12 \Lambda_{ij}^{lm} \mathcal{S}_{lm}^{(3)}(\eta, \boldsymbol{x}), \qquad (A1)$$

where the source term is given by

$$\begin{aligned}\Lambda_{ij}^{ab}S_{ab}^{(3)}(\eta,\boldsymbol{x}) = \Lambda_{ij}^{ab}\Bigg[&12\phi^{(1)}\partial_a\phi^{(1)}\partial_b\phi^{(1)} - \frac{4}{\mathcal{H}}\phi^{(1)'}\partial_a\phi^{(1)}\partial_b\phi^{(1)} + \frac{2}{3\mathcal{H}^2}\Delta\phi^{(1)}\partial_a\phi^{(1)}\partial_b\phi^{(1)}\\ &+ \frac{2}{3\mathcal{H}^4}\Delta\phi^{(1)}\partial_a\phi^{(1)'}\partial_b\phi^{(1)'} - \frac{3}{\mathcal{H}^2}\phi^{(1)'}\partial_a\phi^{(1)'}\partial_b\phi^{(1)} - \frac{3}{\mathcal{H}^2}\phi^{(1)'}\partial_b\phi^{(1)'}\partial_a\phi^{(1)}\\ &+ \frac{2}{3\mathcal{H}^3}\Delta\phi^{(1)}\partial_a\phi^{(1)'}\partial_b\phi^{(1)} + \frac{2}{3\mathcal{H}^3}\Delta\phi^{(1)}\partial_b\phi^{(1)'}\partial_a\phi^{(1)} - \frac{2}{\mathcal{H}^3}\phi^{(1)'}\partial_a\phi^{(1)'}\partial_b\phi^{(1)'} - \frac{4}{\mathcal{H}^2}\phi^{(1)}\partial_a\phi^{(1)'}\partial_b\phi^{(1)'}\\ &- \frac{1}{2}\phi^{(1)}\big(h_{ab}^{(2)''} + 2\mathcal{H}h_{ab}^{(2)'} - \Delta h_{ab}^{(2)}\big) - \phi^{(1)}\Delta h_{ab}^{(2)} - \phi^{(1)'}\mathcal{H}h_{ab}^{(2)} - \frac{1}{3}\Delta\phi^{(1)}h_{ab}^{(2)} - \partial^c\phi^{(1)}\partial_c h_{ab}^{(2)}\\ &+ \phi^{(1)}\partial_a\big(V_b^{(2)'} + 2\mathcal{H}V_b^{(2)}\big) + \phi^{(1)}\partial_b\big(V_a^{(2)'} + 2\mathcal{H}V_a^{(2)}\big) + \phi^{(1)'}\big(\partial_a V_b^{(2)} + \partial_b V_a^{(2)}\big)\\ &- \frac{\phi^{(1)}}{8\mathcal{H}}\big(\partial_b\Delta V_a^{(2)} + \partial_a\Delta V_b^{(2)}\big) - \frac{\phi^{(1)'}}{8\mathcal{H}^2}\big(\partial_b\Delta V_a^{(2)} + \partial_a\Delta V_b^{(2)}\big) + \frac{1}{\mathcal{H}}\big(\phi^{(1)}\partial_a\partial_b\psi^{(2)'}\big)\\ &+ \frac{1}{\mathcal{H}}\big(\phi^{(1)'}\partial_a\partial_b\phi^{(2)}\big) + \frac{1}{\mathcal{H}^2}\big(\phi^{(1)'}\partial_a\partial_b\psi^{(2)'}\big) + 3\big(\phi^{(1)}\partial_a\partial_b\phi^{(2)}\big)\Bigg].\end{aligned} \tag{A2}$$

Third-order gravitational waves are produced by both the linear scalar perturbations and second-order metric perturbations that are produced by the linear scalar perturbations. The latter were studied in the literature [30,83].

In Fourier space, the evolution of the first- and second-order metric perturbations is given by

$$\phi_{\boldsymbol{k}}^{(1)} = \Phi_{\rm k}T_\phi(k\eta), \tag{A3a}$$

$$\phi_{\boldsymbol{k}}^{(2)} = \int\frac{{\rm d}^3k}{(2\pi)^3}\{\Phi_{\boldsymbol{k}-\boldsymbol{p}}\Phi_{\boldsymbol{p}}I_\phi(|\boldsymbol{k}-\boldsymbol{p}|,|\boldsymbol{p}|,k\eta)\}, \tag{A3b}$$

$$\psi_{\boldsymbol{k}}^{(2)} = \int\frac{{\rm d}^3k}{(2\pi)^3}\{\Phi_{\boldsymbol{k}-\boldsymbol{p}}\Phi_{\boldsymbol{p}}I_\psi(|\boldsymbol{k}-\boldsymbol{p}|,|\boldsymbol{p}|,k\eta)\}, \tag{A3c}$$

$$V_{i,\boldsymbol{k}}^{(2)} = \int\frac{{\rm d}^3k}{(2\pi)^3}\left\{\Phi_{\boldsymbol{k}-\boldsymbol{p}}\Phi_{\boldsymbol{p}}\mathcal{V}_i^{ab}\frac{p_ap_b}{k^2}I_V(|\boldsymbol{k}-\boldsymbol{p}|,|\boldsymbol{p}|,k\eta)\right\}, \tag{A3d}$$

$$h_{ij,\boldsymbol{k}}^{(2)} = \int\frac{{\rm d}^3k}{(2\pi)^3}\left\{\Phi_{\boldsymbol{k}-p}\Phi_{\boldsymbol{p}}\Lambda_{ij}^{ab}\frac{p_ap_b}{k^2}I_h(|\boldsymbol{k}-\boldsymbol{p}|,|\boldsymbol{p}|,k\eta)\right\}, \tag{A3e}$$

where $\mathcal{V}_j^{ab}(\boldsymbol{k}) = -ik_j(\delta^{ab}-k^ak^b/k^2)/k^2$ is helicity decomposition operator for vector perturbations, $\Lambda_{ij}^{ab}(\boldsymbol{k}) = \frac{1}{2}[(\delta_i^b - k^bk_i/k^2)(\delta_j^a-k^ak_j/k^2) + (\delta_i^a-k^ak_i/k^2)(\delta_j^b-k^bk_j/k^2) - (\delta^{ab}-k^ak^b/k^2)(\delta_{ij}-k_ik_j/k^2)]$ is that for tensor perturbations [31], and $\Phi_{\boldsymbol{k}}$ is a stochastic variable characterizing the primordial scalar perturbations. During radiation domination, the initial conditions lead to $\Phi_{\boldsymbol{k}} = 2\zeta_{\boldsymbol{k}}/3$, where $\zeta_{\boldsymbol{k}}$ denotes primordial curvature perturbations with wave vector $\boldsymbol{k}$. The transfer function T_ϕ is obtained by solving the master equation for the linear scalar perturbations [84]. As shown in Ref. [30], the kernel functions I_ϕ, I_ψ, I_V, and I_h are obtained by solving the equations of motion for $\phi^{(2)}$, $\psi^{(2)}$, $V^{(2)}$, and $h^{(2)}$, respectively.

In Fourier space, Eq. (A2) is reformulated as

$$\begin{aligned}\Lambda_{ij}^{ab}(\boldsymbol{k})S_{ab,\boldsymbol{k}}^{(3)} = &\,\mathbb{P}_{(\phi^{(1)})^3,ij}(\boldsymbol{k},\boldsymbol{p},\boldsymbol{q})f_1\big[\phi_{\boldsymbol{k}-\boldsymbol{p}}^{(1)},\phi_{\boldsymbol{p}-\boldsymbol{q}}^{(1)},\phi_{\boldsymbol{q}}^{(1)}\big] + \mathbb{P}_{\phi^{(1)}h^{(2)},ij}(\boldsymbol{k},\boldsymbol{p},\boldsymbol{q})f_2\big[\phi_{\boldsymbol{k}-\boldsymbol{p}}^{(1)},\Phi_{\boldsymbol{p}-\boldsymbol{q}}\Phi_{\boldsymbol{q}}I_h(|\boldsymbol{p}-\boldsymbol{q}|,|\boldsymbol{q}|,|\boldsymbol{p}|\eta)\big]\\ &+ \mathbb{P}_{\phi^{(1)}V^{(2)},ij}(\boldsymbol{k},\boldsymbol{p},\boldsymbol{q})f_3\big[\phi_{\boldsymbol{k}-\boldsymbol{p}}^{(1)},\Phi_{\boldsymbol{p}-\boldsymbol{q}}\Phi_{\boldsymbol{q}}I_V(|\boldsymbol{p}-\boldsymbol{q}|,|\boldsymbol{q}|,|\boldsymbol{p}|\eta)\big]\\ &+ \mathbb{P}_{\phi^{(1)}\psi^{(2)},ij}(\boldsymbol{k},\boldsymbol{p},\boldsymbol{q})f_4\big[\phi_{\boldsymbol{k}-\boldsymbol{p}}^{(1)},\Phi_{\boldsymbol{p}-\boldsymbol{q}}\Phi_{\boldsymbol{q}}I_\psi(|\boldsymbol{p}-\boldsymbol{q}|,|\boldsymbol{q}|,|\boldsymbol{p}|\eta)\big],\end{aligned} \tag{A4}$$

where $f_n[...]$ with $n = 1, 2, 3, 4$ are homogeneous functions of order 1, that can be read straightforwardly from Eq. (A2), and we introduce

$$\mathbb{P}_{(\phi^{(1)})^3,ij}(\boldsymbol{k},\boldsymbol{p},\boldsymbol{q}) = \frac{1}{k^2}\Lambda_{ij}^{ab}(\boldsymbol{k})[(p_a-q_a)q_b + (p_b-q_b)q_a], \tag{A5a}$$

$$\mathbb{P}_{\phi^{(1)}\psi^{(2)},ij}(\boldsymbol{k},\boldsymbol{p},\boldsymbol{q}) = \frac{1}{k^2}\Lambda_{ij}^{ab}(\boldsymbol{k})p_ap_b, \tag{A5b}$$

$$\mathbb{P}_{\phi^{(1)}V^{(2)},ij}(\boldsymbol{k},\boldsymbol{p},\boldsymbol{q}) = \frac{1}{k^2}\Lambda_{ij}^{ab}(\boldsymbol{k})\big[\mathcal{V}_a^{cd}(\boldsymbol{p})q_cq_dp_b + \mathcal{V}_b^{cd}(\boldsymbol{p})q_cq_dp_a\big], \tag{A5c}$$

$$\mathbb{P}_{\phi^{(1)}h^{(2)},ij}(\boldsymbol{k},\boldsymbol{p},\boldsymbol{q}) = \frac{1}{k^2}\Lambda_{ij}^{ab}(\boldsymbol{k})\Lambda_{ab}^{cd}(\boldsymbol{p})q_cq_d. \tag{A5d}$$

Solving Eq. (A1) in Fourier space, we get the strain of third-order gravitational waves as

$$h^{(3)}_{ij,\boldsymbol{k}} \equiv \int \frac{\mathrm{d}^3p}{(2\pi)^3}\frac{\mathrm{d}^3q}{(2\pi)^3}\Big\{\Phi_{\boldsymbol{k}-\boldsymbol{p}}\Phi_{\boldsymbol{p}-\boldsymbol{q}}\Phi_{\boldsymbol{q}}\Big[\mathbb{P}_{(\phi^{(1)})^3,ij}(\boldsymbol{k},\boldsymbol{p},\boldsymbol{q})I^{(3)}_{(\phi^{(1)})^3}(|\boldsymbol{k}-\boldsymbol{p}|,|\boldsymbol{p}-\boldsymbol{q}|,|\boldsymbol{q}|,|\boldsymbol{p}|,k,\eta) + \mathbb{P}_{\phi^{(1)}h^{(2)},ij}(\boldsymbol{k},\boldsymbol{p},\boldsymbol{q})I^{(3)}_{\phi^{(1)}h^{(2)}}(|\boldsymbol{k}-\boldsymbol{p}|,|\boldsymbol{p}-\boldsymbol{q}|,|\boldsymbol{q}|,|\boldsymbol{p}|,k,\eta) + \mathbb{P}_{\phi^{(1)}V^{(2)},ij}(\boldsymbol{k},\boldsymbol{p},\boldsymbol{q})I^{(3)}_{\phi^{(1)}V^{(2)}}(|\boldsymbol{k}-\boldsymbol{p}|,|\boldsymbol{p}-\boldsymbol{q}|,|\boldsymbol{q}|,|\boldsymbol{p}|,k,\eta) + \mathbb{P}_{\phi^{(1)}\psi^{(2)},ij}(\boldsymbol{k},\boldsymbol{p},\boldsymbol{q})I^{(3)}_{\phi^{(1)}\psi^{(2)}}(|\boldsymbol{k}-\boldsymbol{p}|,|\boldsymbol{p}-\boldsymbol{q}|,|\boldsymbol{q}|,|\boldsymbol{p}|,k,\eta)\Big]\Big\}, \tag{A6}$$

where the kernel functions $I^{(3)}_{*}(|\boldsymbol{k}-\boldsymbol{p}|,|\boldsymbol{p}-\boldsymbol{q}|,|\boldsymbol{q}|,|\boldsymbol{p}|,k,\eta)$ are defined as

$$I^{(3)}_{(\phi^{(1)})^3} = \int_0^\eta \mathrm{d}\bar{\eta}G_k(\eta,\bar{\eta})f_1[T_\phi(|\boldsymbol{k}-\boldsymbol{p}|\bar{\eta}),T_\phi(|\boldsymbol{p}-\boldsymbol{q}|\bar{\eta}),T_\phi(|\boldsymbol{q}|\bar{\eta})], \tag{A7a}$$

$$I^{(3)}_{\phi^{(1)}h^{(2)}} = \int_0^\eta \mathrm{d}\bar{\eta}G_k(\eta,\bar{\eta})f_2[T_\phi(|\boldsymbol{k}-\boldsymbol{p}|\bar{\eta}),I_h(|\boldsymbol{p}-\boldsymbol{q}|,|\boldsymbol{q}|,|\boldsymbol{p}|\bar{\eta})], \tag{A7b}$$

$$I^{(3)}_{\phi^{(1)}V^{(2)}} = \int_0^\eta \mathrm{d}\bar{\eta}G_k(\eta,\bar{\eta})f_3[T_\phi(|\boldsymbol{k}-\boldsymbol{p}|\bar{\eta},I_V(|\boldsymbol{p}-\boldsymbol{q}|,|\boldsymbol{q}|,|\boldsymbol{p}|\bar{\eta})], \tag{A7c}$$

$$I^{(3)}_{\phi^{(1)}\psi^{(2)}} = \int_0^\eta \mathrm{d}\bar{\eta}G_k(\eta,\bar{\eta})f_4[T_\phi(|\boldsymbol{k}-\boldsymbol{p}|\bar{\eta}),I_\psi(|\boldsymbol{p}-\boldsymbol{q}|,|\boldsymbol{q}|,|\boldsymbol{p}|\bar{\eta})], \tag{A7d}$$

with the Green's function during radiation domination being

$$G_k(\eta,\bar{\eta}) = \frac{1}{k}\sin[k(\eta-\bar{\eta})]. \tag{A8}$$

There is not a kernel function with a subscript $\phi^{(1)}\phi^{(2)}$, since $\phi^{(2)}$ has been replaced with $\psi^{(2)}$ via the second-order equation of motion.

[1] K. N. Ananda, C. Clarkson, and D. Wands, The cosmological gravitational wave background from primordial density perturbations, Phys. Rev. D **75**, 123518 (2007).

[2] D. Baumann, P. J. Steinhardt, K. Takahashi, and K. Ichiki, Gravitational wave spectrum induced by primordial scalar perturbations, Phys. Rev. D **76**, 084019 (2007).

[3] S. Mollerach, D. Harari, and S. Matarrese, CMB polarization from secondary vector and tensor modes, Phys. Rev. D **69**, 063002 (2004).

[4] H. Assadullahi and D. Wands, Constraints on primordial density perturbations from induced gravitational waves, Phys. Rev. D **81**, 023527 (2010).

[5] J. Espinosa, D. Racco, and A. Riotto, A cosmological signature of the SM Higgs instability: Gravitational waves, J. Cosmol. Astropart. Phys. **2018**, 012 (2018).

[6] K. Kohri and T. Terada, Semianalytic calculation of gravitational wave spectrum nonlinearly induced from primordial curvature perturbations, Phys. Rev. D **97**, 123532 (2018).

[7] H. Xu *et al.*, Searching for the nano-Hertz stochastic gravitational wave background with the Chinese pulsar timing array data release I, Res. Astron. Astrophys. **23**, 075024 (2023).

[8] J. Antoniadis *et al.*, The second data release from the European Pulsar Timing Array, III. Search for gravitational wave signals, Astron. Astrophys. **678**, A50 (2023).

[9] G. Agazie *et al.* (NANOGrav), The NANOGrav 15-year data set: Evidence for a gravitational-wave background, Astrophys. J. Lett. **951**, L8 (2023).

[10] D. J. Reardon *et al.*, Search for an isotropic gravitational-wave background with the Parkes Pulsar Timing Array, Astrophys. J. Lett. **951**, L6 (2023).

[11] J. Antoniadis *et al.*, The second data release from the European Pulsar Timing Array: V. Implications for massive black holes, dark matter and the early universe, arXiv:2306.16227.

[12] A. Afzal *et al.* (NANOGrav), The NANOGrav 15-year data set: Search for signals from new physics, Astrophys. J. Lett. **951**, L11 (2023).

[13] G. Agazie *et al.* (NANOGrav), The NANOGrav 15-year data set: Constraints on supermassive black hole binaries from the gravitational wave background, arXiv:2306.16220.

[14] G. Franciolini, A. Junior Iovino, V. Vaskonen, and H. Veermae, The recent gravitational wave observation by pulsar timing arrays and primordial black holes: The importance of non-Gaussianities, Phys. Rev. Lett. **131**, 201401 (2023).

[15] K. Inomata, K. Kohri, and T. Terada, The detected stochastic gravitational waves and sub-solar primordial black holes, arXiv:2306.17834.

[16] S. Wang, Z.-C. Zhao, J.-P. Li, and Q.-H. Zhu, Exploring the implications of 2023 pulsar timing array datasets for scalar-induced gravitational waves and primordial black holes, arXiv:2307.00572.

[17] L. Liu, Z.-C. Chen, and Q.-G. Huang, Implications for the non-Gaussianity of curvature perturbation from pulsar timing arrays, arXiv:2307.01102.

[18] K. T. Abe and Y. Tada, Translating nano-Hertz gravitational wave background into primordial perturbations taking account of the cosmological QCD phase transition, Phys. Rev. D **108**, L101304 (2023).

[19] R. Ebadi, S. Kumar, A. McCune, H. Tai, and L.-T. Wang, Gravitational waves from stochastic scalar fluctuations, arXiv:2307.01248.

[20] D. G. Figueroa, M. Pieroni, A. Ricciardone, and P. Simakachorn, Cosmological background interpretation of pulsar timing array data, arXiv:2307.02399.

[21] Z. Yi, Q. Gao, Y. Gong, Y. Wang, and F. Zhang, The waveform of the scalar induced gravitational waves in light of pulsar timing array data, Sci. China-Phys. Mech. Astron. **66**, 120404 (2023).

[22] E. Madge, E. Morgante, C. P. Ibáñez, N. Ramberg, and S. Schenk, Primordial gravitational waves in the nano-Hertz regime and PTA data–Towards solving the GW inverse problem, J. High Energy Phys. 03 (2023) 171.

[23] Y.-F. Cai, X.-C. He, X. Ma, S.-F. Yan, and G.-W. Yuan, Limits on scalar-induced gravitational waves from the stochastic background by pulsar timing array observations, Sci. Bull. **68**, 2929 (2023).

[24] M. Maggiore, *Gravitational Waves, Vol. 2: Astrophysics and Cosmology* (Oxford University Press, Oxford, England, 2018).

[25] C. J. Moore and A. Vecchio, Ultra-low-frequency gravitational waves from cosmological and astrophysical processes, Nat. Astron. **5**, 1268 (2021).

[26] T. L. Smith, E. Pierpaoli, and M. Kamionkowski, A new cosmic microwave background constraint to primordial gravitational waves, Phys. Rev. Lett. **97**, 021301 (2006).

[27] T. J. Clarke, E. J. Copeland, and A. Moss, Constraints on primordial gravitational waves from the cosmic microwave background, J. Cosmol. Astropart. Phys. **2020**, 002 (2020).

[28] R. Cooke, M. Pettini, R. A. Jorgenson, M. T. Murphy, and C. C. Steidel, Precision measures of the primordial abundance of deuterium, Astrophys. J. **781**, 31 (2014).

[29] C. Yuan, Z.-C. Chen, and Q.-G. Huang, Probing primordial–black-hole dark matter with scalar induced gravitational waves, Phys. Rev. D **100**, 081301(R) (2019).

[30] J.-Z. Zhou, X. Zhang, Q.-H. Zhu, and Z. Chang, The third order scalar induced gravitational waves, J. Cosmol. Astropart. Phys. **2022**, 013 (2022).

[31] Z. Chang, S. Wang, and Q.-H. Zhu, Note on gauge invariance of second order cosmological perturbations, Chin. Phys. C **45**, 095101 (2021).

[32] P. Ivanov, P. Naselsky, and I. Novikov, Inflation and primordial black holes as dark matter, Phys. Rev. D **50**, 7173 (1994).

[33] J. Garcia-Bellido, A. D. Linde, and D. Wands, Density perturbations and black hole formation in hybrid inflation, Phys. Rev. D **54**, 6040 (1996).

[34] J. Yokoyama, Chaotic new inflation and formation of primordial black holes, Phys. Rev. D **58**, 083510 (1998).

[35] Y.-F. Cai, X. Tong, D.-G. Wang, and S.-F. Yan, Primordial black holes from sound speed resonance during inflation, Phys. Rev. Lett. **121**, 081306 (2018).

[36] Y.-F. Cai, C. Chen, X. Tong, D.-G. Wang, and S.-F. Yan, When primordial black holes from sound speed resonance meet a stochastic background of gravitational waves, Phys. Rev. D **100**, 043518 (2019).

[37] R.-G. Cai, Z.-K. Guo, J. Liu, L. Liu, and X.-Y. Yang, Primordial black holes and gravitational waves from parametric amplification of curvature perturbations, J. Cosmol. Astropart. Phys. **2020**, 013 (2020).

[38] C. Chen and Y.-F. Cai, Primordial black holes from sound speed resonance in the inflaton-curvaton mixed scenario, J. Cosmol. Astropart. Phys. **2019**, 068 (2019).

[39] C. Chen, X.-H. Ma, and Y.-F. Cai, Dirac-Born-Infeld realization of sound speed resonance mechanism for primordial black holes, Phys. Rev. D **102**, 063526 (2020).

[40] Y.-H. Yu and S. Wang, Anisotropies in scalar-induced gravitational-wave background from inflaton-curvaton mixed scenario with sound speed resonance, arXiv:2310.14606.

[41] S. Wang, T. Terada, and K. Kohri, Prospective constraints on the primordial black hole abundance from the stochastic gravitational-wave backgrounds produced by coalescing events and curvature perturbations, Phys. Rev. D **99**, 103531 (2019); **101**, 069901(E) (2020).

[42] N. Aghanim *et al.* (Planck), Planck 2018 results. VI. Cosmological parameters, Astron. Astrophys. A **641**, 6 (2020); (Planck), Planck 2018 results. VI. Cosmological parameters, Astron. Astrophys. **652**, C4(E) (2021).

[43] K. Saikawa and S. Shirai, Primordial gravitational waves, precisely: The role of thermodynamics in the standard model, J. Cosmol. Astropart. Phys. **2018**, 035 (2018).

[44] P. Campeti, E. Komatsu, D. Poletti, and C. Baccigalupi, Measuring the spectrum of primordial gravitational waves with CMB, PTA and laser interferometers, J. Cosmol. Astropart. Phys. **2021**, 012 (2021).

[45] D. Poletti, Measuring the primordial gravitational wave background in the presence of other stochastic signals, J. Cosmol. Astropart. Phys. **2021**, 052 (2021).

[46] T. Bringmann, P. F. Depta, T. Konstandin, K. Schmidt-Hoberg, and C. Tasillo, Does NANOGrav observe a dark sector phase transition? arXiv:2306.09411.

[47] P. E. Dewdney, P. J. Hall, R. T. Schilizzi, and T. J. L. W. Lazio, The square kilometre array, Proc. IEEE **97**, 1482 (2009).

[48] A. Weltman *et al.*, Fundamental physics with the Square Kilometre Array, Publ. Astron. Soc. Aust. **37**, e002 (2020).

[49] C. J. Moore, R. H. Cole, and C. P. L. Berry, Gravitational-wave sensitivity curves, Class. Quantum Grav. **32**, 015014 (2015).

[50] A. Sesana *et al.*, Unveiling the gravitational universe at μ-Hz frequencies, Exper. Astron. **51**, 1333 (2021).

[51] P. Amaro-Seoane *et al.* (LISA), Laser Interferometer Space Antenna, arXiv:1702.00786.

[52] T. Robson, N. J. Cornish, and C. Liu, The construction and use of LISA sensitivity curves, Class. Quantum Grav. **36**, 105011 (2019).

[53] J. Crowder and N. J. Cornish, Beyond LISA: Exploring future gravitational wave missions, Phys. Rev. D **72**, 083005 (2005).

[54] G. M. Harry, P. Fritschel, D. A. Shaddock, W. Folkner, and E. S. Phinney, Laser interferometry for the big bang observer, Class. Quantum Grav. **23**, 4887 (2006); **23**, 7361 (2006).

[55] S. Sato *et al.*, The status of DECIGO, J. Phys.: Conf. Ser. **840**, 012010 (2017).

[56] S. Kawamura *et al.*, Current status of space gravitational wave antenna DECIGO and B-DECIGO, Prog. Theor. Exp. Phys. **2021**, 05A105 (2021).

[57] M. Punturo *et al.*, The Einstein Telescope: A third-generation gravitational wave observatory, Class. Quantum Grav. **27**, 194002 (2010).

[58] G. M. Harry (LIGO Scientific), Advanced LIGO: The next generation of gravitational wave detectors, Class. Quantum Grav. **27**, 084006 (2010).

[59] F. Acernese *et al.* (VIRGO), Advanced Virgo: A second-generation interferometric gravitational wave detector, Class. Quantum Grav. **32**, 024001 (2015).

[60] K. Somiya (KAGRA), Detector configuration of KAGRA: The Japanese cryogenic gravitational-wave detector, Class. Quantum Grav. **29**, 124007 (2012).

[61] Z.-C. Zhao and S. Wang, Bayesian implications for the primordial black holes from NANO Grav's pulsar-timing data using the scalar-induced gravitational waves, Universe **9**, 157 (2023).

[62] K. Schmitz, New sensitivity curves for gravitational-wave signals from cosmological phase transitions, J. High Energy Phys. 01 (2021) 097.

[63] K. Abazajian *et al.*, CMB-S4 science case, reference design, and project plan, arXiv:1907.04473.

[64] P. Ade *et al.* (Simons Observatory), The Simons Observatory: Science goals and forecasts, J. Cosmol. Astropart. Phys. **2019**, 056 (2019).

[65] E. Allys *et al.* (LiteBIRD), Probing cosmic inflation with the LiteBIRD cosmic microwave background polarization survey, Prog. Theor. Exp. Phys. **2023**, 042F01 (2023).

[66] B. Carr, K. Kohri, Y. Sendouda, and J. Yokoyama, Constraints on primordial black holes, Rep. Prog. Phys. **84**, 116902 (2021).

[67] N. Kitajima, J. Lee, K. Murai, F. Takahashi, and W. Yin, Nanohertz gravitational waves from axion domain walls coupled to QCD, arXiv:2306.17146.

[68] S.-Y. Guo, M. Khlopov, X. Liu, L. Wu, Y. Wu, and B. Zhu, Footprints of axion-like particle in Pulsar Timing Array data and JWST observations, arXiv:2306.17022.

[69] Y. Gouttenoire and E. Vitagliano, Domain wall interpretation of the PTA signal confronting black hole overproduction, arXiv:2306.17841.

[70] C. Unal, A. Papageorgiou, and I. Obata, Axion-gauge dynamics during inflation as the origin of pulsar timing array signals and primordial black holes, arXiv:2307.02322.

[71] Y. Gouttenoire, S. Trifinopoulos, G. Valogiannis, and M. Vanvlasselaer, Scrutinizing the primordial black holes interpretation of PTA gravitational waves and JWST early galaxies, arXiv:2307.01457.

[72] H.-L. Huang, Y. Cai, J.-Q. Jiang, J. Zhang, and Y.-S. Piao, Supermassive primordial black holes in multiverse: For nano-Hertz gravitational wave and high-redshift JWST galaxies, arXiv:2306.17577.

[73] P. F. Depta, K. Schmidt-Hoberg, and C. Tasillo, Do pulsar timing arrays observe merging primordial black holes? arXiv:2306.17836.

[74] C. Han, K.-P. Xie, J. M. Yang, and M. Zhang, Self-interacting dark matter implied by nano-Hertz gravitational waves, arXiv:2306.16966.

[75] S. Choudhury, S. Panda, and M. Sami, Quantum loop effects on the power spectrum and constraints on primordial black holes, JCAP **11**, 066 (2023).

[76] K. Batygin and M. E. Brown, Evidence for a distant giant planet in the solar system, Astron. J. **151**, 22 (2016).

[77] K. Batygin, F. C. Adams, M. E. Brown, and J. C. Becker, The planet nine hypothesis, Phys. Rep. **805**, 1 (2019).

[78] C. A. Trujillo and S. S. Sheppard, A Sedna-like body with a perihelion of 80 astronomical units, Nature (London) **507**, 471 (2014).

[79] J. Scholtz and J. Unwin, What if Planet 9 is a primordial black hole? Phys. Rev. Lett. **125**, 051103 (2020).

[80] P. Mróz, A. Udalski, J. Skowron, R. Poleski, S. Kozłowski, M. K. Szymański, I. Soszyński, Ł. Wyrzykowski, P. Pietrukowicz, K. Ulaczyk, D. Skowron, and M. Pawlak, No large population of unbound or wide-orbit Jupiter-mass planets, Nature (London) **548**, 183 (2017).

[81] H. Niikura, M. Takada, S. Yokoyama, T. Sumi, and S. Masaki, Constraints on Earth-mass primordial black holes from OGLE 5-year microlensing events, Phys. Rev. D **99**, 083503 (2019).

[82] E. Witten, Searching for a black hole in the outer solar system, arXiv:2004.14192.

[83] K. Inomata, Analytic solutions of scalar perturbations induced by scalar perturbations, J. Cosmol. Astropart. Phys. **2021**, 013 (2021).

[84] S. Dodelson, *Modern Cosmology* (Academic Press, London, 2003).